JOURNAL OF MATERIALS SCIENCE 12 (1977) 353–357

X-ray surface reflection and transmission topography of magnetic domain walls in Czochralski-grown nickel single crystals

MASAO KURIYAMA, WILLIAM J. BOETTINGER, HAROLD E. BURDETTE
Institute for Materials Research, National Bureau of Standards, Washington, D.C., USA

Ferromagnetic domain walls are observed in large Czochralski-grown nickel single crystals by X-ray double crystal diffraction topography in the surface reflection geometry as well as in the transmission geometry. The images of magnetic domain walls in surface reflection topographs possess almost as good contrast as those in transmission topographs, and even reveal fine detailed structure. Based on preliminary arguments, the images observed in the surface reflection topographs are attributed to 180° walls intersecting the crystal surface obliquely, while the transmission topographs easily image 71° and 109° walls in the interior of the crystals.

1. Introduction

X-ray diffraction topography was applied by several authors more than a decade ago to observe ferromagnetic domain walls in different materials using a variety of X-ray optical arrangements [1–4]. Since then extensive studies have been made on the arrangements of domains and domain walls in Fe–Si single crystals by Polcarová *et al.* [5–9], Roessler *et al.* [10–12], Kuriyama and McManus [13], Schlenker and Kleman [14], Miltat and Kleman [15] and Miltat [16]. The domain arrangements in iron single crystals have also been studied extensively by Chikaura *et al.* [17–19], and Yamashita and Mihara [20].

By contrast, there are few X-ray topographic studies of ferromagnetic domains and domain walls in other basic ferromagnetic metals such as nickel. When compared with iron, nickel has smaller saturation magnetization, larger magnetostriction and a substantially smaller magnetic anisotropy energy. These properties can assist in understanding the mechanism of image formations in X-ray dynamical diffraction topography. Nickel crystals would deviate more significatntly from cubic symmetry than iron or iron–silicon crystals. The magnetic domain walls would be broader since the wall thickness is inversely proportional to the square root of magnetic anisotropy energy [21].

The primary difficulty of X-ray topographic observation of magnetic domains and domain walls in nickel crystals lies in the fact that the level of perfection of nickel crystals has usually been insufficient. Below the required degree of crystal perfection, X-ray dynamical diffraction effects such as Borrmann anomalous transmission cannot become predominant. This difficulty has been demonstrated previously by Chikaura *et al.* [22] and Alex *et al.* [23]. Recently, the present authors have succeeded in achieving such a sufficiently high level of crystal perfection in large nickel single crystals grown by the Czochralski technique [24, 25]. The purpose of this paper is to present distinct images of magnetic domain walls in nickel single crystals obtained by X-ray diffraction topography both in the surface reflection geometry and in the transmission geometry. A preliminary discussion will be presented on the types of magnetic domain walls which can be imaged in surface reflection topographs.

2. Experimental procedures

The procedure of nickel single crystal growth and sample preparation for X-ray topography has been described in detail previously [24]. In this paper, only the experimental conditions relevant to the present work are described. The crystal boules

grown were about 12 cm long with diameters between 1.5 and 2.5 cm and with a bottle-neck diameter of slightly less than 1 mm. The boules were sliced into discs with an acid saw and the discs were polished on an acid polishing wheel. For this work, the discs were prepared to have $(1\bar{1}0)$ planes as their parallel faces.

X-ray diffraction topographs were taken both in the surface reflection and in the transmission geometry with an asymmetric (double) crystal topographic (ACT) camera [26, 27]. Cu$K\alpha_1$ radiation was used throughout this work. To avoid damage to the crystals caused by conventional measuring techniques, the thicknesses of the nickel discs were determined by the anomalous transmission effect from the separation between the undiffracted beam and the transmitted (**O**-diffracted) beam in a manner described previously [27]. The thickness of the crystal disc used for the transmission geometry ranged from 0.24 mm at the periphery to 0.45 mm at the centre. The product of the ordinary linear absorption coefficient, $\mu = 47.9\,\text{mm}^{-1}$, and thickness, L, is thus between 11.5 and 21.6.

3. Results

Fig. 1 shows a $2\bar{2}0$ diffraction topograph of a nickel single crystal disc taken with the ACT in the surface reflection geometry. There is a set of long distinct line images running parallel to the $[11\bar{1}]$ direction and another set of shorter and less distinct line images in the [111] direction. Each line image also contains a fine structure in it. The contrast of the images varies from black (fewer photons) to white (more photons) depending upon their location. Contrast can be changed from black to white or vice versa by changing the glancing angle. Also seen is the contrast created by very few crystal imperfections and *very* small angle subgrain boundaries.

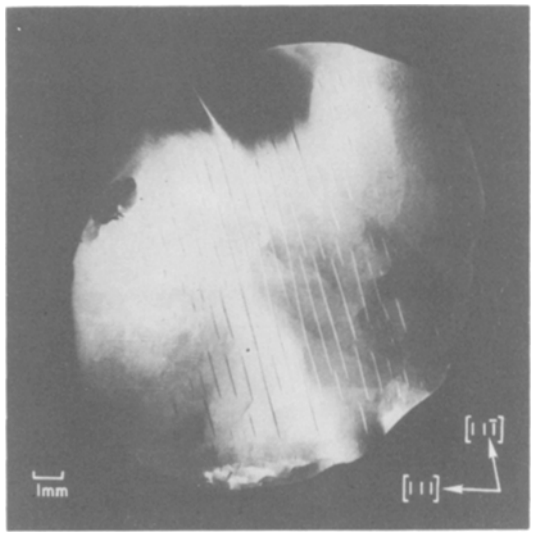

Figure 1 ACT $2\bar{2}0$ surface reflection topograph of a nickel single crystal showing long straight line images parallel to $[11\bar{1}]$ and short line images parallel to [111].

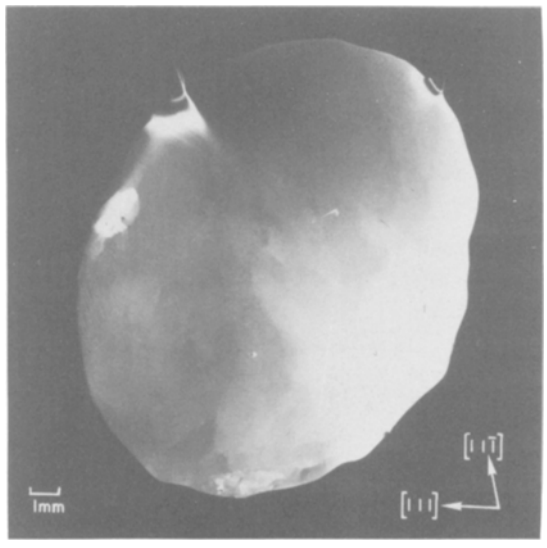

Figure 2 ACT $2\bar{2}0$ surface reflection topograph of the same nickel crystal as shown in Fig. 1 with a magnetic field of 2.39×10^4 A m^{-1} applied parallel to $[11\bar{1}]$. The line images parallel to $[11\bar{1}]$ and [111] have disappeared.

When a magnetic field of 2.39×10^4 Am^{-1}* is applied in one of the easy directions of magnetization, [111], the line images disappear completely as shown in Fig. 2. The images related to subgrain boundaries and crystal imperfections have remained unchanged. In such magnetic fields, crystals are magnetized to a single domain. Note that this topograph as well as the previous one has revealed the entire shape of the crystal disc with the strain sensitive ACT system. This topograph has, therefore, indicated that this nickel crystal possesses a high quality of crystal perfection.

Fig. 3 shows $11\bar{1}$ transmission topographs taken from a different crystal disc, for which the value of μL ranges from 11.5 to 21.6, as described in Section 2. A topograph of the **O**-diffracted (transmitted) beam is shown in Fig. 3a and that of the **H**-diffracted (Bragg-diffracted) beam in Fig.

*1 A m^{-1} $= 4\pi \times 10^{-3}$ Oe.

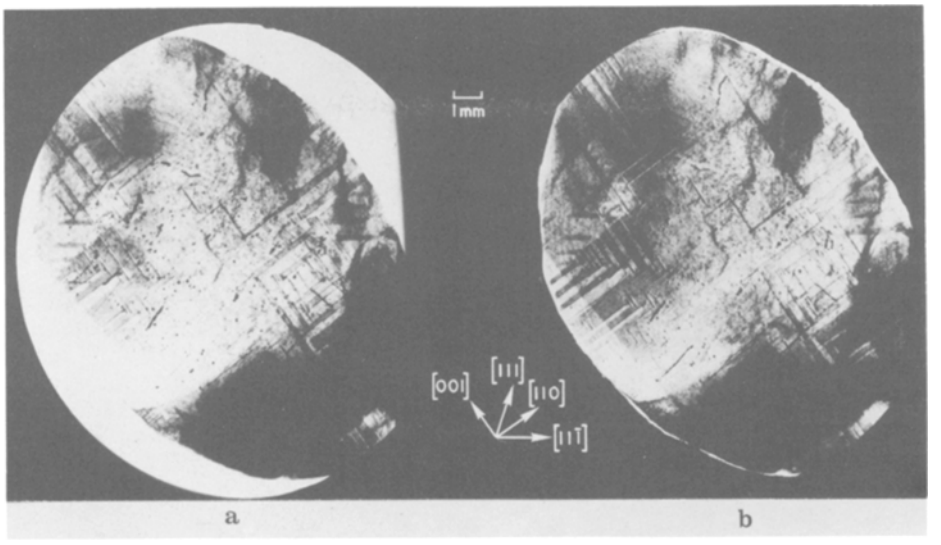

Figure 3 ACT 11$\bar{1}$ transmission topograph of a nickel single crystal with μL between 11.5 and 21.6. Note the rectangular arrangements of straight line images parallel to [001] and [110].

3b. A lighter (white) area indicates that more photons have reached this area, while a dark (black) area implies that photons have been disrupted by the crystal. Most of the details in both topographs a and b are identical; in particular the disruption images [28, 29] caused by crystal imperfections such as dislocations and dislocation clusters match perfectly with each other. It should be noted again that the topographs have revealed the entire exposed shape of the crystal disc, indicating that anomalous transmission effects have occurred throughout the crystal. Upon the application of a magnetic field in an easy magnetization direction, the regular straight line images and the rectangular image arrangements disappear as reported in separate papers [24, 25].

At the top area of the topographs there is a set of fine straight line disruption images which are spaced densely and run perpendicular to the [111] direction. These images are immediately recognized as those of glissile dislocations* similar to dislocations frequently created by slight deformation in perfect copper crystals [30]. A majority of regular images in the topographs consists of straight line images forming rectangular arrangements. The directions of these lines are either [001] or [110], in contrast with the directions of the images observed in the surface reflection topograph. In addition to these distinct images, sets of black band images are seen at both right and left side areas. These bands run parallel to the [11$\bar{1}$] direction.

4. Discussion

It was thought, in the past, that surface reflection topography was not appropriate to observe magnetic domains or domain walls even close to crystal surfaces, unless the magnetostriction was large enough to produce diffracted beams from different mosaic blocks which could be resolved [1]. Although Polcarová and Kaczer [5] and Reed *et al.* [31] obtained topographs of magnetic domains in Fe–Si single crystals with the surface reflection geometry, their image contrast was not as appreciable as that in the transmission geometry. To our knowledge, Fig. 1 is, perhaps, the first surface reflection topograph of magnetic domain walls almost as distinct and well-resolved as those obtained in the transmission geometry. It should naturally be noted that surface diffraction topographs only reveal the image of objects lying near the surface, while transmission topographs can reveal structures in the interior of crystals.

Although the domain configurations can be quite complex, we will attempt to present a plausible explanation for the images in the surface

*By the application of contrast conditions with different diffracting planes, these glissile dislocations are easily distinguished from sessile dislocations, whose appearance is very similar in topographs to that of glissile dislocations [27, 30].

reflection topograph. For this discussion, let us assume that the magnetization vectors in the sample crystals lie in directions of easy magnetization, [111] and [11$\bar{1}$] in the (1$\bar{1}$0) plane which is parallel to the surfaces of the crystal disc. In such crystals, 71° and 109° domain walls intersect the crystal surfaces in lines parallel to [001] and [110], while 180° walls intersect the crystal surfaces in lines parallel to [111] and [11$\bar{1}$]. These possible wall directions coincide with the directions of the observed images; the images in the surface reflection topograph possibly represent the 180° walls, while the majority of the images in the transmission topographs represent the 71° and/or 109° walls.* On the basis of possible magnetic flux configurations, many 180° walls must be present in the crystal shown in Fig. 3. Yet these images are not visible, nor are they visible on the surface reflection topographs of this crystal.† Except for the domain walls which are imaged as a band, all the domain walls in Fig. 3 are perpendicular to the surface; the 71° and 109° walls can be imaged by the strain inside the walls, while the 180° walls cannot be imaged because of the negligible strain in the wall. This is consistent with observations made in Fe and Fe–Si, that 180° walls seldom form images in X-ray transmission topographs.

However, when the 180° walls make an angle with the surfaces of a nickel single crystal, nonvanishing strains may be induced in the wall, resulting in the dark band images as seen in Fig. 3. When this geometry occurs, the 180° walls intersecting the surfaces may create a significant local strain distribution near the surface and produce the diffraction contrast as observed in the surface reflection topograph, Fig. 1. On the other hand, the walls perpendicular to the surface may not strain the surface area anymore than they do in the interior of the crystals. Surface reflection topographs have thus been shown to augment information obtained from transmission topographs about the nature of magnetic domain arrangements.

Acknowledgement

The work reported herein was partially supported by the Advanced Missions Program of the National Aeronautics and Space Administration. The authors wish to express their thanks to Roberta M. Eaton and Deborah A. Lavin of the Metallurgy Division, National Bureau of Standards for their technical assistance.

References

1. K. M. MERTZ, *J. Appl. Phys.* **31** (1960) 147.
2. M. POLCAROVÁ and A. R. LANG, *Appl. Phys. Letters* **1** (1962) 13.
3. B. ROESSLER, J. J. KRAMER and M. KURIYAMA, *Phys. Stat. Sol.* **11** (1965) 117.
4. J. BASTERFIELD and M. J. PRESCOTT, *J. Appl. Phys.* **38** (1967) 3190.
5. M. POLCAROVÁ and J. KACZER, *Phys. Stat. Sol.* **21** (1967) 635.
6. M. POLCAROVÁ and J. GEMPERLOVÁ, *ibid* **32** (1969) 769.
7. M. POLCAROVÁ and A. R. LANG, *ibid* (*a*) **4** (1971) 491.
8. J. BRÁDLER and M. POLCAROVÁ, *ibid* (*a*) **9** (1972) 179.
9. M. POLCAROVA, *Z. Naturforsch.* **28a** (1973) 639.
10. B. ROESSLER, *Phys. Stat. Sol.* **20** (1967) 713.
11. C. WU and B. ROESSLER, *ibid* (*a*) **8** (1971) 571.
12. *Idem, J. Appl. Phys.* **42** (1971) 1814.
13. M. KURIYAMA and G. M. McMANUS, *Phys. Stat. Sol.* **25** (1968) 667.
14. M. SCHLENKER and M. KLEMAN, *J. Phys.* **32** (1971) C1-256.
15. J. E. MILTAT and M. KLEMAN, *Phil. Mag.* **28** (1973) 1015.
16. J. E. MILTAT, *ibid* **33** (1976) 225.
17. S. NAGAKURA and Y. CHIKAURA, *J. Phys. Soc. Japan* **30** (1971) 495.
18. Y. CHIKAURA, T. MORI and S. NAGAKURA, *ibid* **35** (1973) 404.
19. Y. CHIKAURA, *Jap. J. Appl. Phys.* **15** (1976) 385.
20. T. YAMASHITA and A. MIHARA, *ibid* **10** (1971) 1661.
21. C. KITTEL, *Rev. Mod. Phys.* **21** (1949) 541.
22. Y. CHIKAURA, H. FUKUMORI and S. NAGAKURA, *Jap. J. Appl. Phys.* **11** (1972) 1582.
23. V. ALEX, L. V. TIKHONOV and O. BRÜMMER, *Kristal u. Technik* **9** (1974) 643.
24. M. KURIYAMA, W. J. BOETTINGER and H. E. BURDETTE, NBS IR 76-980 (1976) 3.
25. *Idem, J. Appl. Phys.* **47** (11) (1976).
26. W. J. BOETTINGER, H. E. BURDETTE, M. KURIYAMA and R. E. GREEN, JUN., *Rev. Sci. Instrum.* **47** (1976) 906.
27. M. KURIYAMA, J. G. EARLY and H. E. BURDETTE, *J. Appl. Cryst.* **1** (1974) 535.

*Some of the short line segment images in Fig. 3 possibly have a width almost as wide as a magnetic domain itself. Their image contrast, however, is probably created by the image contrast of the narrowly spaced walls.

†A few short line segment images of the ⟨111⟩ directions are, however, seen, consistent with Fig. 1, at the locations where the dark band images appear in the transmission topograph.

28. M. KURIYAMA, *Phil. Mag.* **34** (1976) 119.
29. *Idem, ibid* **A25** (1969) 681
30. W. J. BOETTINGER, H. E. BURDETTE and M. KURIYAMA, *Phil. Mag.* **34** (1976) 119.
31. R. E. REED, E. D. BOLLING and H. E. HARMON, Annual Progress Report (Oak Ridge National Laboratory) ORNL-4952 (1973) p. 129.
Received 26 April and accepted 28 May 1976.